Biosensors and Bioelectronics 77 (2016) 687–694

Contents lists available at ScienceDirect

Biosensors and Bioelectronics

journal homepage: www.elsevier.com/locate/bios

Sensitive detection of *Escherichia coli* O157:H7 using Pt–Au bimetal nanoparticles with peroxidase-like amplification

Tao Jiang [a,c,1], Yang Song [a,1], Tianxiang Wei [a], He Li [a], Dan Du [a,d], Mei-Jun Zhu [b,*], Yuehe Lin [a,d,*,**]

[a] School of Mechanical and Material Engineering, Washington State University, Pullman, WA 99164, United States
[b] School of Food Science, Washington State University, Pullman, WA 99164, United States
[c] Key Laboratory of Animal Virology of Ministry of Agriculture, State Key Laboratory of Veterinary Etiological Biology, Lanzhou Veterinary Research Institute, Chinese Academy of Agricultural Sciences, Lanzhou, Gansu 730046, China
[d] Paul G. Allen School for Global Animal Health, Washington State University, Pullman, WA 99164, United States

ARTICLE INFO

Article history:
Received 1 July 2015
Received in revised form
15 September 2015
Accepted 6 October 2015
Available online 8 October 2015

Keywords:
Immunochromatographic assay
Pathogens detection
Pt–Au nanoparticles
Peroxidase
E. coli O157:H7

ABSTRACT

Escherichia coli O157:H7 is one of the most notorious foodborne pathogens causing serious disease at low infectious dose. To protect consumers from deadly foodborne *E. coli* O157:H7 infection, it is vital to develop a simple, reliable, sensitive and rapid method which can detect low level *E. coli* O157:H7 in foods at real-time. We have successfully developed a novel immunochromatographic assay (ICA) with enhanced sensitivity for the visual and quantitative detection of *E. coli* O157:H7. Sandwich-type immunoreactions were performed on the ICA, and Pt–Au bimetal nanoparticles (NPs) were accumulated on the test zone. The signal amplification is based on Pt–Au bimetal NPs possessing high peroxidase activity toward 3,3′,5,5′-tetramethylbenzidine, which can produce characteristic colored bands and thus, enable visual detection of *E. coli* O157:H7 without instrumentation. The innovative aspect of this approach lies in the visualization and quantification of target pathogen through the detection of color intensity. Due to the excellent peroxidase activity of Pt–Au NPs, they emit strong visible color intensity in less than 1 min for visual observation even in low concentration range of *E. coli* O157:H7. Quantification was performed using a commercial assay meter. The sensitivity was improved more than *1000-folds* compared to the conventional test strip based on colored gold-colloids. Although the feasibility was demonstrated using *E. coli* O157:H7 as a model analyte, this approach could be easily developed to be a universal signal amplification technique and applied to detection of a wide variety of foodborne pathogens and protein biomarkers.

1. Introduction

Escherichia coli O157:H7 is an important foodborne pathogen that has low infectious dose and causes serious illness in humans including with bloody diarrhea and hemolytic uremic syndrome and even death. Enterohemorrhagic *E. coli* (EHEC) cause more than 63,000 illnesses, 2100 hospitalizations and 20 deaths each year in the United States. Of which, *E. coli* O157:H7 is the main EHEC serotype that causes the majority of EHEC human infections. *E. coli* O157:H7 is involved in a variety of foodborne outbreaks associated with ground beef, fresh produce, rice cakes, dairy products and others (Marder et al., 2014; Nabae et al., 2013; Jacob et al., 2013; McCollum et al., 2012; Scallan et al., 2011; Wendel et al., 2009; Riley et al., 1983). At present, USDA has a zero tolerance policy to control *E. coli* O157:H7 contamination in ground beef. Additionally, along with *Salmonella* spp. and *Listeria monocytogenes,* (FDA, 2015, CDC, 2012b, CDC, 2012a), *E. coli* O157:H7 foodborne outbreak has been an emerging issue for fresh produce, as reflected in nationwide *E. coli* O157:H7 spinach outbreaks sickened more than 200 people and killed 3 people (CDC, 2006). In response to low infectious dose and devastating consequences of fresh produce outbreak, the FDA Food Safety Modernization Act targets the safety of fresh and minimally processed foods. Hence, developing a rapid, sensitive, and accurate method to detect *E. coli* O157:H7 in various foods with complex matrix and extreme pH is crucial in preventing disastrous *E. coli* O157:H7 outbreaks and associated human infection. The expanding requirements for reliable diagnostic techniques of infectious agents (Kirsch et al., 2013; Kiilerich-

* Corresponding author.
** Corresponding author at: School of Mechanical and Material Engineering, Washington State University, Pullman, WA 99164, United States.
E-mail addresses: meijun.zhu@wsu.edu (M.-J. Zhu), yuehe.lin@wsu.edu (Y. Lin).
[1] T. Jiang and Y. Song are equally contributed to this work.

http://dx.doi.org/10.1016/j.bios.2015.10.017
0956-5663/

Pedersen et al., 2011; Miranda et al., 2011; Vikesland and Wigginton, 2010; Dover et al., 2009; Sampath et al., 2007) in food have attracted intensive attentions to develop varieties of diagnostic strategies, such as cell phone based diagnostics (Khan et al., 2013), new kind of fluorescence signal amplification reporters (Chi et al., 2012; Mannoor et al., 2012; Huang et al., 2011; Li et al., 2010; Zou et al., 2010) and various kinds of nanomaterials based biosensors (Sun et al., 2015; Eksi et al., 2015; Yazgan et al., 2014; Li et al., 2014; Liu et al., 2014). As one of the most promising assays for point of care diagnostic, immunochromatographic assay (ICA) is widely used at individual pregnancy diagnosis. The principle of ICA is a sandwich immunoreaction. After the sample was added to the membrane, it started to react with captured antibody (Ab1) to form complex, which began to pass along the nitrocellulose membrane by capillary action until reaching the detection antibody (Ab2) in the test zone to achieve the sandwich immunoreaction. ICA outweighs the most common assays, such as bacterial culture (Sack and Sack, 1975), PCR (Cebula et al., 1995), loopmediated amplification (LAMP) (Kinoshita et al., 2015; Wang et al., 2014, 2012b) and ELISA (Liu et al., 2008), because of its low cost, easy operation, rapid, quantitative detection and accuracy (Zhang et al., 2014b; Liu et al., 2014, 2007; Du et al., 2012; Peng et al., 2007).

Colloidal golds served as labels to develop ICA has been applied for the detection of branches of analysts because of its high level of photo brightness, promising chemical stability and strong biocompatibility (Mao et al., 2008; Nagatani et al., 2006); whereas the detection limit of most reported ones cannot detect low levels of foodborne pathogens or infectious agents (Zhang et al., 2015; Xie et al., 2014a; Karakus and Salih, 2013; Shen et al., 2011; Qi et al., 2011; Chiao et al., 2004; Shyu et al., 2002). Thus, great efforts have been made to improve the sensitivity of ICA using different labels (Zhu et al., 2015c, 2015b; Chen et al., 2014; Ge et al., 2014; Zhang et al., 2013; Liu et al., 2012, 2011; Lin et al., 2008). ICA utilizing nanomaterials such as quantum dots (Roda et al., 2012), bioconjugated nanoparticles (NPs) probe (Kalele et al., 2006; Zhao et al., 2004), colored latex particles and up-converting phosphors (Shan et al., 2015; Zhang et al., 2014a, Corstjens et al., 2014, Imai et al., 1993), exhibits higher detection sensitivity and broader response range than colloidal gold based conventional ICA. However, the increased sensitivity brings out several drawbacks. Their chemical instability, expensive instruments requirements and long handling time limit them from facilitating quantitative analysis in food industry at real time (Xu et al., 2010; Resch-Genger et al., 2008; Ulrich et al., 2008; Wang et al., 2005). Also, the industrial authority usually regards rapid bacterial detection as a method which can be done within fifty minutes. Therefore, it is extremely critical to establish a low cost, rapid and ultrasensitive method with systematic signal amplification protocol for visually pathogen detection.

With the high surface area, diversified composition and excellent electron conductivity, the porous bimetallic NPs have provided excellent catalytic performance and have been addressed as promising nanomaterial in decades in biomedical research (Zhu et al., 2015a; Wang et al., 2012a; Lehoux et al., 2012; Guo and Wang, 2011; Xu et al., 2009). For instance, the Pt or Au based bimetallic NPs have been broadly utilized in biomedical field because of strong catalytic activity and unique biocompatibility (Ma et al., 2011; Xiao et al., 2009; Zeng et al., 2006). Specifically, Pt based NPs is the most research-attractive material because of its wide application in catalysis, sensing, biomedical diagnosis and therapy, etc. (Hu et al., 2014; Maiyalagan et al., 2012). Additionally, porous bimetal NPs usually exhibit better thermo-stability than enzymes, which require appropriate condition to keep their three dimension structures for their functionality. Hence, these specific characters offer great potential in developing ICA to detect foodborne pathogen in food and food processing environments, which usually have a very complicated matrix and acidity, capable of inhibiting enzymatic reaction.

Herein, we report a novel Pt–Au NPs based ICA for easy-operation and rapid detection of *E. coli* O157:H7 with high sensitivity resulting from the amplification of peroxidase activity of Pt–Au NPs. 3,3′,5,5′-Tetramethylbenzidine (TMB), a chromogenic reagent, served as a good signal amplifier because it could be catalyzed by Pt–Au NPs producing blue color products, which provides higher visible sensitivity than other classic substrates (He et al., 2011). Under the optimal condition, the detection limit of new device is 10^2 cells mL^{-1}, which was about 1/1000 of the recent conventional colloidal based ICA (10^5 cells mL^{-1}, Wang et al., 2006). Experimental results demonstrated that the Pt–Au based ICA provides a reliable, rapid, sensitive strategy for visual detection of pathogen. Pt–Au based ICA has a great potential for point of care application in clinical diagnostics and food industry.

2. Experimental section

2.1. Materials and chemistry

E. coli O157:H7 EDL933 was obtained from the STEC center at Michigan State University. The strain was stored in Luria Broth (LB, Fisher Scientific, Pittsburgh, PA) medium containing 15% glycerol at −80 °C, and was activated in LB broth at 37 °C overnight with aeration.

Horseradish peroxidase (HRP), 3,3′,5,5′-Tetramethylbenzidine (TMB), TMB Liquid Substrate System for ELISA which contains concentration of H_2O_2, Pluronic F127, K_2PtCl_4 (Pt, 44.99%), $HAuCl_4$ (Au, 49.98%), commercial Pt carbon nanopowder, hydrochloric acid (HCl, 39%), polyvinylpyrrolidone (PVP), sodium hydroxide (NaOH) and ascorbic acid were purchased from Sigma-Aldrich. Fetal bovine serum (FBS) and bovine serum albumin (BSA) were purchased from ATCC. Mouse anti-*E. coli* O157:H7 polyclonal antibody (Ab1), mouse anti-*E. coli* O157:H7 monoclonal antibody (Ab2) were purchased from Kirkegaard & Perry Laboratories Inc (Baltimore, MD). Nitrocellulose membrane, fiber sample pad, fiber conjugate pad, laminated cards, and absorbent pad were used by provided. Ultrapure water from Millipore Milli-Q water purification system was used for experiments. The phosphate buffered saline (PBS) containing Na_2HPO_4 and NaH_2PO_4 was prepared using de-ionized water (18.2 MΩ cm), and the pH was adjusted with NaOH and H_3PO_4. All the reagents are analytical standard and used without further purification.

2.2. E. coli O157:H7 sample preparation

Overnight *E. coli* O157:H7 cultures were washed with 1 × PBS, pH 7.0 and re-suspended in 1 × PBS. Portion of washed *E. coli* O157:H7 suspension was serial diluted and proper dilutions were plated on LB agar plates for cell enumeration. The remaining *E. coli* O157:H7 suspension was heated in 95 °C water bath for 30 min, then formalin was added to a final concentration of 0.5% (v/v). Mortalized *E. coli* O157:H7 were used for safety reasons and to ensure a static (non-proliferating) sample population for quantitative purposes.

2.3. Preparation of porous Pt–Au NPs

Pt–Au NPs was synthesized as previously described (Ataee-Esfahani et al., 2013) with slight modifications. Pluronic F127 (10 mg) was ultrasonically dissolved into 1.0 mL of aqueous solution containing K_2PtCl_4 (20 mM), $HAuCl_4$ (20 mM) and HCl (6 M). After adding 1.0 mL of ascorbic acid (100 mM), the reducing agent,

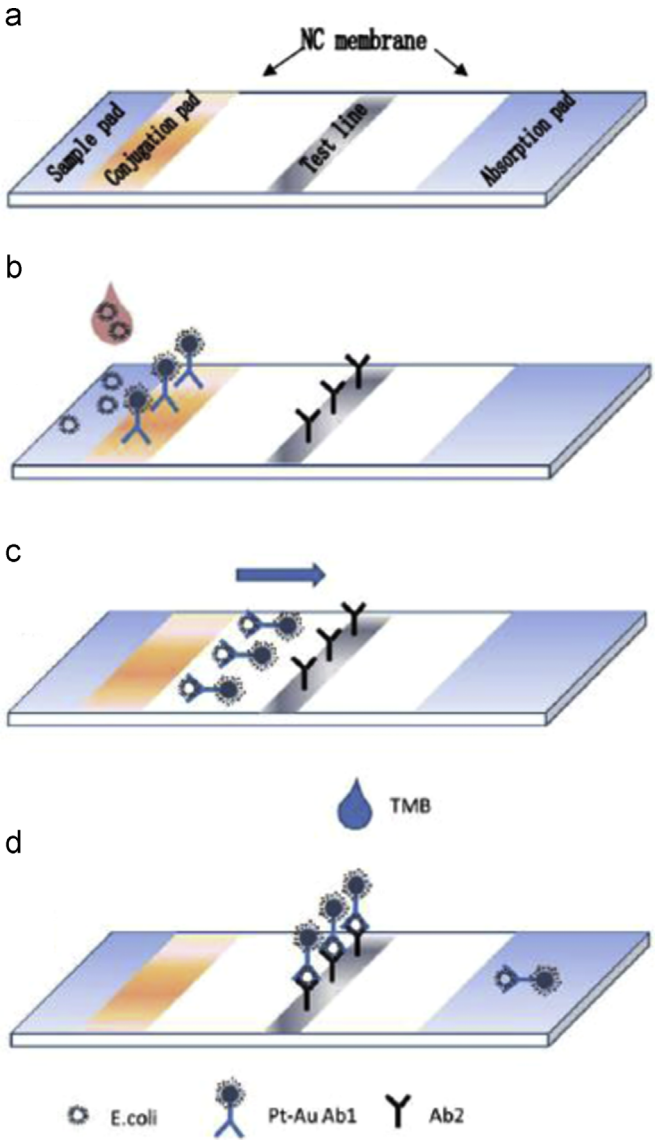

Scheme 1. Schematic illustration of ICA platform detection of *E. coli* O157:H7 (a–d). (a) Typical assembly of ICA. The ICA system consists of sample pad, conjugated pad, adsorption pad and nitrocellulose membrane. All components are bound together layer-by-layer. (b). The anti-*E. coli* O157:H7 Ab1 was covalent bounded with Pt–Au NPs and then modified onto the conjugated pad. *E. coli* O157:H7 is applied to the sample pad. (c) *E. coli* O157:H7 combines with Pt–Au–anti-*E. coli* O157:H7 Ab1 conjugates and migrates along the porous membrane by capillary action. (d) The formed complexes continue to migrate along the membrane and are captured by the monoclonal antibodies (Ab2) to form Pt–Au–Ab1-*E. coli*- Ab2 complexes on the test line. As the liquid sample continues migrating, the excess complexes are migrated toward the absorption pad. Signal was amplified by adding TMB at test line.

the mixture was continuously sonicated in a water bath for 0.5 h, and then reacted with a magnetic stirrer for 24 h at 30 °C. The final product was collected and washed with acetone and water in consecutive washing/centrifugation cycles five times and then dried at room condition.

2.4. Preparation of Pt–Au-capture antibody (Ab1)

The pH of the Pt–Au NPs solution was optimized by adding 0.02 M K_2CO_3 before the capture antibody was added. Desired weight of capture antibody was mixed with desired amount of Pt–Au NPs, followed by gentle shaking for 1 h at room temperature. Then, 10 wt% BSA was added to a final concentration of 1% BSA, and the mixture was incubated for 30 min. The mixture was further washed with PBS with 1% BSA and centrifuged at 8000 rpm for 10 min. The prepared Pt–Au-capture antibody conjugates were collected and suspended in eluent buffer (pH 7.4, containing 10 mM PBS, 0.25% Tween-20, 10% sucrose, and 5% BSA). The total volume of solution after dissolving equals one tenth of the volume of the pervious solution of Pt–Au-capture antibody conjugates.

2.5. Preparation of assay

Scheme 1 illustrates the test strip components schematically. The sample pad was pretreated with blocking buffer containing 10 mM PBS, 0.1% (w/v) Tween-20, and 1% (wt/v) PVP, pH 7.4. Pt–Au–antibody conjugates were dispensed onto the conjugated pad. Desired volume of mouse monoclonal anti- *E. coli* O157:H7 antibody solution (0.8 mg mL^{-1}, Ab_2) was dispensed on the reaction membrane to form the test zone, and then was pretreated with blocking buffer. All the parts mentioned have to be dried 2 h at 37 °C before assembled on a plastic adhesive backing card, which was cut into 4 mm strips and stored at room condition.

2.6. Assay procedure

50 μL of the analyte (*E. coli* O157:H7) was dropped onto the sample pad and diffused through the reaction membrane driven by the capillary force, which enabled the reaction with Ab1-labeled Pt–Au NPs to form complex at conjugation pad. The yielding complex then passed along the nitrocellulose membrane by capillary action until reaching the Ab2 in the test line to achieve the sandwich immunoreaction. After adding TMB, the final signal intensity on test line was observed and quantified using a test strip reader after the immunoreaction finishing.

2.7. Instruments and characterization

The transmission electron microscopy (TEM) was conducted with Philips CM200UT. The scan electron microscopy (SEM) was conducted using FEI Quanta 200F. The Energy Dispersive X-ray Spectrameter (EDX) was obtained with FEI Quanta 200F. X-ray photoelectron spectroscopy (XPS) measurements were recorded on a Kratos AXIS-165 multi-technique electron spectrometer system with a base pressure of 1×10^{-9} Torr. XPS were obtained on an AXIS-165 manufactured by Kratos Analytical Inc. (Spring Valley, NY, USA) using a monochromatic X-ray radiation of 1487 eV (Al Ka). The spectrometer was calibrated against both the Au 4f7/2 peak at 84.0 eV and the Ag 3d5/2 peak at 368.3 eV. Static charging when present was corrected with a neutralizer (flood gun) by placing the carbon peak (C 1s) at about 285 eV. A portable fluorescence strip reader ESE-Quant GOLD was purchased from DCN Inc. (Irvine, CA).

3. Result and discussion

3.1. Characteristics of Pt–Au porous nanocolloids

Metal precursors can be reduced simultaneously by a strong reducing agent in liquid phase to form faceted crystal morphology, which is one practicable way to synthesize metallic alloy nanostructures. Additionally, self-assembly of surfactants into spherical micelles can employ faceted crystal as templates to synthesize porous metal NPs. The resulting bimetallic porous Pt–Au nanocolloids provide high surface area with abundant activity sites on the concave surface.

SEM and TEM were performed to characterize the morphology of Pt–Au porous NPs. The average size of NPs is around 50 nm.

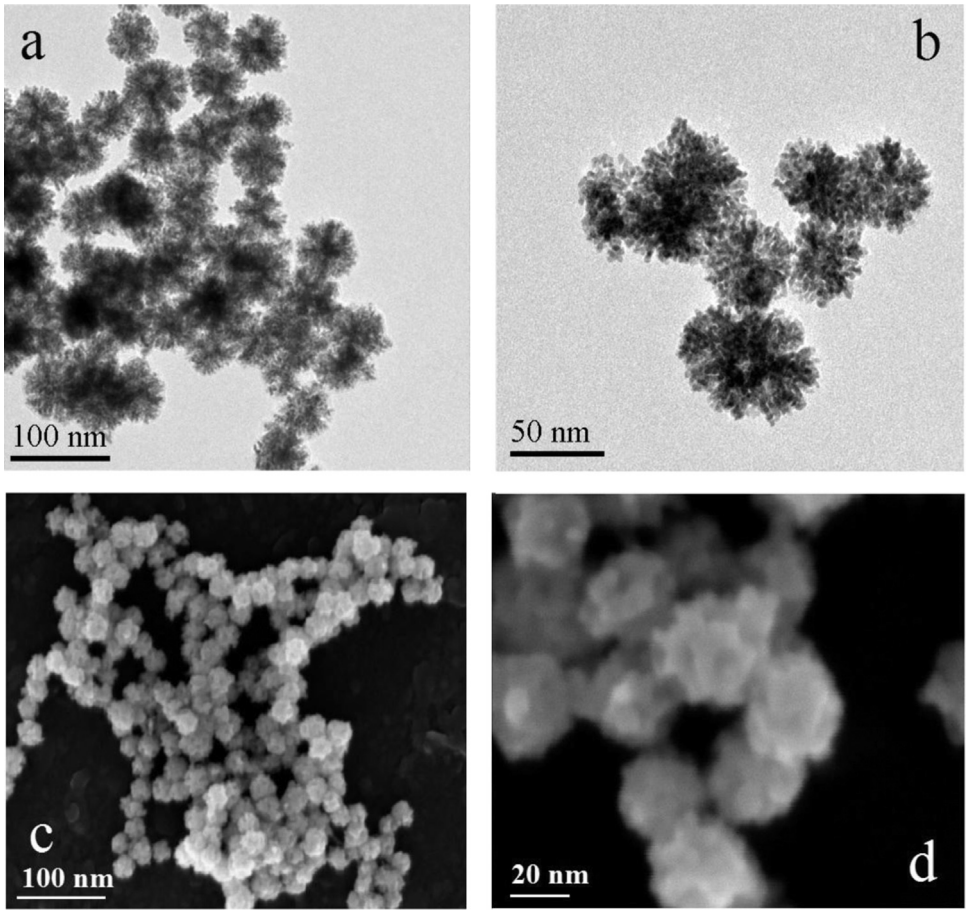

Fig. 1. Electronic microscopic images of Pt–Au porous NPs. (a) TEM; (b) zoom in image of a; (c) SEM; (d) zoom in image for c.

There is a uniform porous structure formed as hemispherical with concavities on the surface of NPs by TEM (Fig. 1a–b). This porous structure was further confirmed by SEM (Fig. 1c–d). The pores are made of fine Pt NPs that form several branched structure on the surface. The Pt NPs had an average diameter of 5 nm and were distributed evenly on the surface of Au NPs.

Furthermore, the formation of NPs was characterized by EDX spectroscopy (Fig. S1a). The corresponding EDX analysis confirmed peaks of presence of elemental Pt and Au in the porous NPs with an atomic Pt:Au ratio of 85.7:9.3, which was close to the stoichiometric ratio of the two metal precursors (9:1). The surface properties were further analyzed by XPS; and the results showing the binding energy of Pt 4f and Au 4f (71.2 eV and 83.3 eV respectively) are consistent with the metallic Pt–Au bimetallic nanostructure and agreed with the result from EDX (Fig. S1b–c).

3.2. Colorimetric analyses of peroxidase-like catalytic activities of Pt–Au NPs

The peroxidase-like catalytic activities of Pt–Au NPs was studied by colorimetric tests using TMB–H_2O_2 substrate. In the presence of H_2O_2, Pt–Au NPs could catalyze H_2O_2-induced TMB oxidation, resulting in a deep blue color solution within 10 min (Fig. 2a). These results indicated that Pt–Au NPs behave as peroxidase toward TMB oxidation with H_2O_2. The relative reaction is described in Fig. 2b, in which H_2O_2 served as electron accepters.

The relationship between the peroxidase-like activity of Pt–Au NPs and H_2O_2 concentrations was further studied (Fig. 2c). The reaction rate strongly depended on the H_2O_2 concentrations while it increased linearly (red line) at low concentration range (0.5–20 mM). This could provide a potential detection method for H_2O_2 related detection. The inset of Fig. 2c is the absorbance evolution for different concentrations of H_2O_2 over time. When increasing the H_2O_2 concentration, the color intensity increased and reached the maximum value at 200 mM.

The peroxidase-like activity of Pt–Au NPs in different concentration ranges was investigated with TMB substrate and H_2O_2, in comparison with commercial Pt nanopowder. The color intensity of the reaction product depends on the Pt–Au NPs concentration ranging from 0.5 to 20 μg mL^{-1}, which is more sensitive than that of Pt nanopowder (Fig. S2a). As shown in Fig. S2b, when the NPs concentration increased from 0 to 20 μg mL^{-1}, the TMB–H_2O_2 assay of Pt–Au NPs achieves higher sensitivity compared to Pt nanopowder. Pt–Au NPs could oxidize more TMB than Pt nanopowder under the same concentration of NPs. These results supported the hypothesis that Pt–Au NPs have stronger peroxidase-like activity than others. The data suggest that the Pt–Au NPs presented a good affinity for H_2O_2. Therefore, the Pt–Au NPs exhibit good catalysis performances, while they could have potential to circumvent intrinsic disadvantages of natural enzyme. Furthermore, the unique surface structure of Pt–Au NPs could significantly improve the surface area and better distribute Pt NPs, which may in turn facilitate greatly improvement of peroxidase-like catalysis activity of Pt–Au NPs.

The thermal and pH stability of Pt–Au NPs were further studied and compared with HRP. Pt–Au NPs exhibited a stable enzymatic catalytic activity toward H_2O_2 in the temperature range from 5 to 90 °C, whereas the enzymatic activity of HRP drastically decreased over 40 °C due to the denaturalization of the enzyme under high temperature (Fig. S3a). Furthermore, Pt–Au NPs exhibited

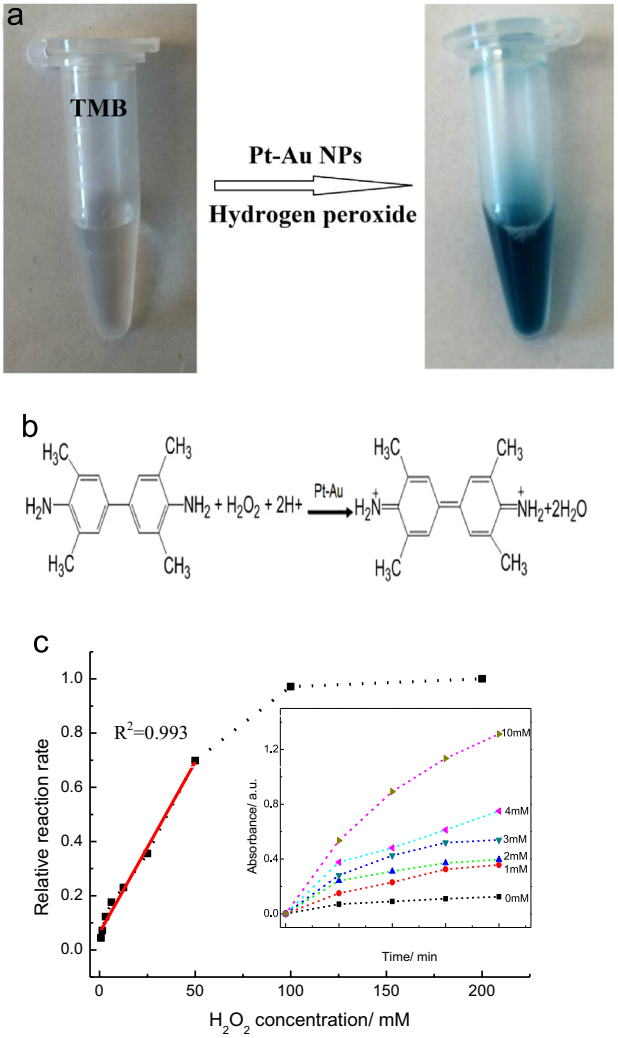

Fig. 2. (a) Color evolution of TMB oxidation in the presence of H_2O_2 in a pH 4.4 PBS buffer. (b) Corresponding reaction mechanisms for H_2O_2 reduction with TMB. (c) Effects of H_2O_2 concentration on the reaction rate of TMB oxidation catalyzed by Pt–Au NPs. The straight line is a linear regression between 0 and 50 mM H_2O_2. The inset is the absorbance evolution at 650 nm over time at various H_2O_2 concentrations.

invariable activity in the solution with the pH range from 2 to 12; whereas the activity of HRP was significantly inhibited when the pH was lower than 7.0 and totally denaturized when pH dropped to 2 (Fig. S3b). Therefore, the demonstrated strong thermal and pH stability of Pt–Au NPs encourages varieties of biological and food applications which have complex matrix and variable pH and require strong and sensitive labels to serve as ultrasensitive reporter.

3.3. Principal of Pt–Au NPs as colored substrates in ICA

Scheme 1 exhibits the schematically configuration and evaluation principle of the Pt–Au based ICA system. Capillary force draws the sample solution onto the dipped ICA. The effort of signal amplification was tested by recording different stages of the reaction of Pt–Au NPs and TMB, shown in Fig. 3. The Pt–Au labeled anti-*E. coli* O157:H7 Ab_1 binds with *E. coli* O157:H7 forming *E. coli*-Pt–Au–Ab_1 complex, and then releases from conjugate area to move through the nitrocellulose membrane until reaches the test zone. Clearly, the color intensity of the test line is proportional to the amount of accumulated Pt–Au NPs in the test zone associating with the *E. coli* O157:H7. The visibility of the dark color test line depends on the concentration of *E. coli* O157:H7 practically. With high concentration of *E. coli* O157:H7 sample (10^6–10^8 cells mL^{-1}), a visible line can be observed; with low concentration, the line could be fuzzy or almost invisible (Fig. 3a). In order to achieve ultrasensitive visual detection, TMB, a chromogenic reagent was used for this purpose. Since TMB can react with Pt–Au NPs resulting in products with blue color, it greatly amplified signal. As shown in Fig. 3b, the clear visible blue lines are shown up even at low concentration range of analyses (10^2–10^5 cells mL^{-1}) when signal-amplification is used. The optical density profiles of both with TMB and without TMB under different concentrations of analyses are shown in Fig. 3c. The ICA with TMB has shown stronger optical intensity and lower detection range than the one without TMB. The results indicate that Pt–Au nanocolloids maintain extreme strong peroxidase activity on ICA and achieve greatly enhanced signal with addition of TMB.

3.4. Pt–Au label based ICA

To examine the signal amplification performance of Pt–Au NPs, the responses of *E. coli* O157:H7 sample in different concentrations (10^2–10^8 cells mL^{-1}) on Pt–Au based ICA assays were obtained and compared with colloidal gold based ICA (Fig. S4). When *E. coli* O157:H7 was not provided in the sample, neither kind of ICA can present any responses in the test zone. There is no colored line shown for colloidal gold based ICA in the case of 10^5 cells mL^{-1} *E. coli* O157:H7 (Fig. S4a), whereas there is a strongly visible blue line in Pt–Au based ICA with TMB (Fig. S4b). There are commercially available test kits such as MaxSignal, RapidChek, Gen-Probe, IQuum, and Watersafe. However, the detection limit ranges from 10^5 to 10^7 cells mL^{-1} without an enrichment step and is $\sim 10^5$ cells mL^{-1} for live *E. coli* O157:H7 (Wang et al., 2006). The detection limit of Pt–Au based ICA was significantly lower than that of colloidal gold based ICA. Visible blue lines were observed at 10^2 cells mL^{-1} of *E. coli* O157:H7 after adding TMB solution as the signal amplifier (Fig. 4b), the intensity enhanced progressively with increasing amount of *E. coli* O157:H7; whereas the colloidal gold based ICA did not show visible signal until *E. coli* O157:H7 concentration reached to 10^6 cells mL^{-1} (Fig. S4a). The dramatic improvement of detection limit (10^2 cells mL^{-1}) for the Pt–Au based ICA is due to its high surface to volume ratio and excellent catalytic activity. In addition, Pt–Au NPs was very high the peroxidase activity, the visual detection can be achieved within a 1 min.

Under optimal experimental conditions, portable test strip reader was used to detect the signal of the Pt–Au based ICA. Fig. 4a and b exhibited the typical photo images and the corresponding optical response recorded by the portable strip reader under different concentrations of *E. coli* O157:H7. No visual test line was observed on the test zone of ICA in the negative control, which revealed a negligible nonspecific adsorption under the optimal experimental conditions. The remarkable blue test lines were seen even at 10^2 cells mL^{-1}, indicating the developed ICA device could serve as a simple visual yes/no determination of *E. coli* O157:H7 without expensive equipment. The peak of intensity or the darkness of the test lines enhanced with the increasing concentration of *E. coli* O157:H7 (Fig. 4a). Furthermore, the peak intensity increased with the increasing concentration of *E. coli* O157:H7. The concentration–peak intensity relationship can be fitted with a log-linear model analysis as shown in the inset of Fig. 4b. By employing the approach of test strips reader, the proposed sensing platform will be estimated as a quantifiable and sensitive strategy for detection of *E. coli* O157:H7. Compared with the conventional colloid gold based *E. coli* O157:H7 ICA, which has a detection limit of 10^6 cells mL^{-1}, the proposed Pt–Au ICA has a lower naked eye detection limit (10^2 cells mL^{-1}), a broader detection range, rapid

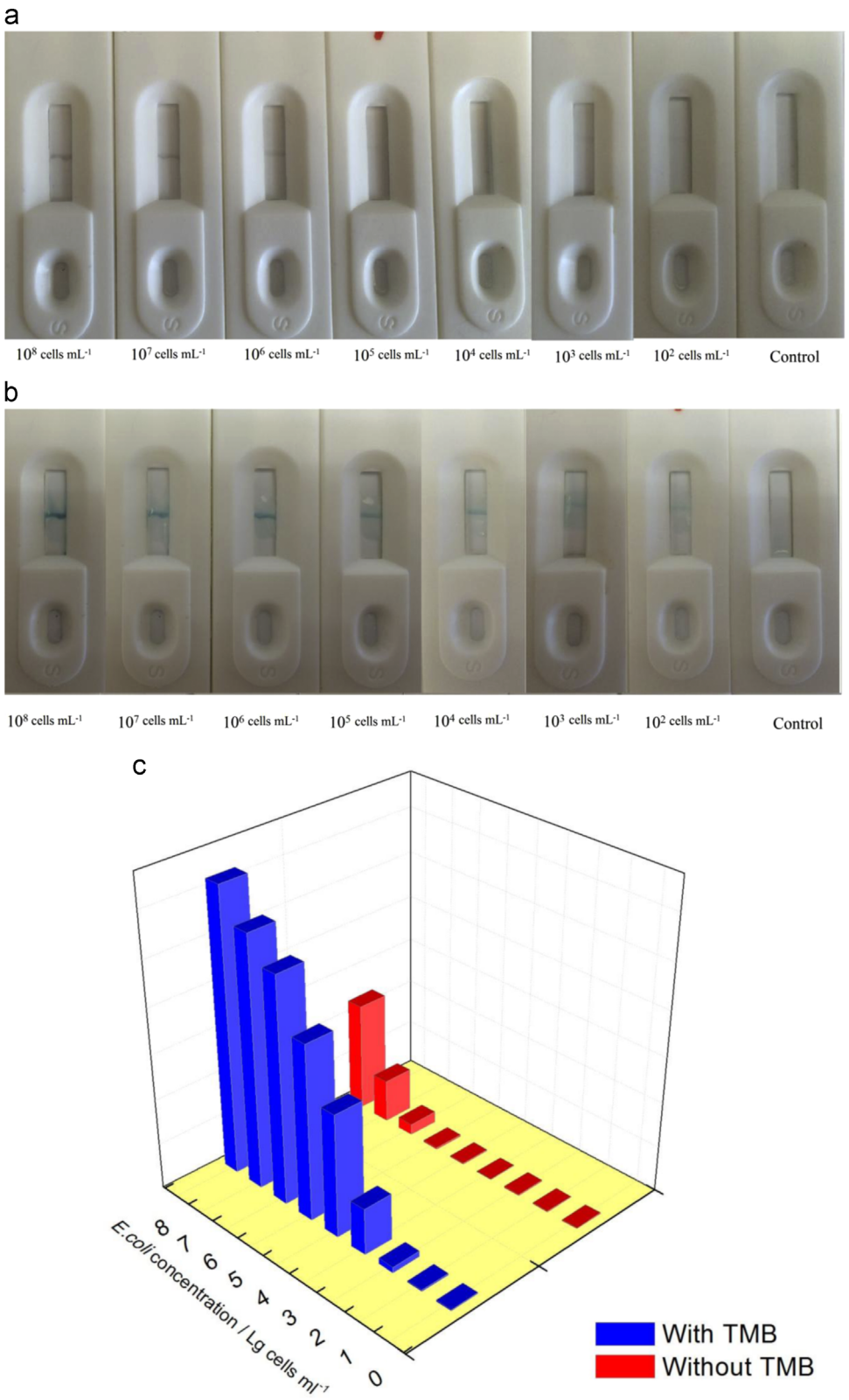

Fig. 3. The photo-images of reaction processes for the Pt–Au based ICA corresponding to different *E. coli* O157:H7 concentrations (from right to left: 10^8 cells mL^{-1}, 10^7 cells mL^{-1}, 10^6 cells mL^{-1}, 10^5 cells mL^{-1}, 10^4 cells mL^{-1}, 10^3 cells mL^{-1}, 10^2 cells mL^{-1} and control). (a) Without TMB: test line was observed only at high concentration range. (b) With TMB: color test lines occurred 5 min after adding TMB even under low *E. coli* O157:H7 concentrations and the test zone turned into blue due to extreme high peroxidase activity. (c) Typical intensity response curves using strip reader corresponding to different *E. coli* O157:H7 concentrations without or with TMB addition.

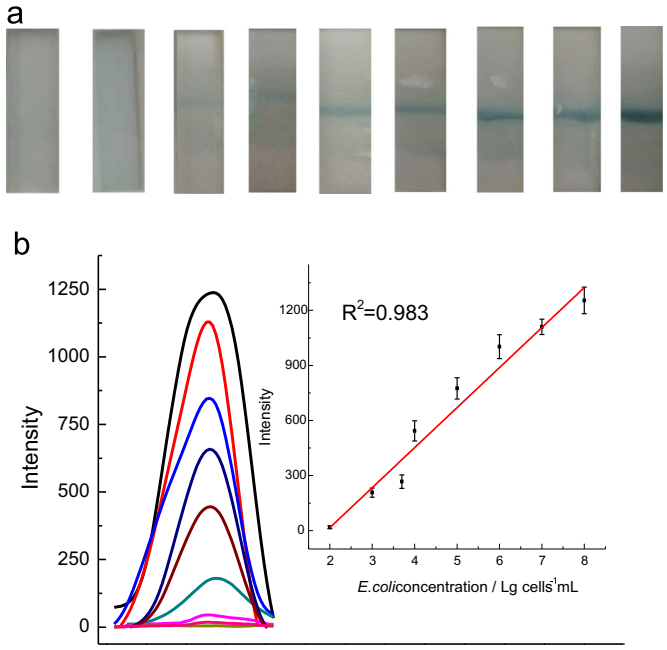

Fig. 4. (a) Typical photo-images for the Pt–Au based ICA corresponding to different *E. coli* O157:H7 concentrations after adding TMB. From left to right, the *E. coli* O157:H7 concentrations are control, 10^1 cells mL^{-1}, 10^2 cells mL^{-1}, 10^3 cells mL^{-1}, 10^4 cells mL^{-1}, 10^5 cells mL^{-1}, 10^6 cells mL^{-1}, 10^7 cells mL^{-1} and 10^8 cells mL^{-1}, respectively. (b) Typical intensity response curves using strip reader corresponding to different *E. coli* O157:H7 concentrations after adding TMB. Inset: The relationship between the concentration of *E. coli* O157:H7 and the test line intensity. Each point represents the average data value obtained from five independent tests.

Table 1
The comparison of ICA used for detection of *E. coli* O157:H7.

	Detection limit (cells mL^{-1})	Refs
Carboxyl-fluorescent microsphere	10^4	(Xie et al., 2014b)
Flower-like Au NPs	10^5	(Zhang et al., 2015)
Magnetic NPs	10^5	(Qi et al., 2011)
Colloidal Au NPs	10^5	(Jung et al., 2005)
Superparamagnetic NPs	10^4	(Shi et al., 2015)
Pt–Au NPs	10^2	This work

detective ability, which can visualize the signal without expensive instruments (Table 1).

3.5. Characterization and optimization of the immunoreaction

The signal to noise ratio (S/N) of ICA, which represents the immunoreaction efficiency and detection sensitivity, is affected by several perspectives: the concentration of Pt–Au NPs conjugated on antibody, the concentration of antibody associating with Pt–Au NPs, the pH of the detection condition, and the reaction time. In addition, the economic cost also influences the selection of optimal condition.

The S/N ratio increased up to 20 μg mL^{-1} of Pt–Au NPs conjugated on antibody because of the increasing Pt–Au NPs captured by those antibodies (Fig. S5a). After that, the S/N ratio decreased again due to the increasing residual NPs attributing to the increasing background noise (Fig. S5a). Hence, 20 μg mL^{-1} of Pt–Au NPs was adopted for all the following experiments.

Up to 13 μg mL^{-1} antibody, the S/N ratio increased as the concentration of antibody increased (Fig. S5b). The increasing antibody enhanced the immunoreaction efficiency contributing to the stronger signal. As 13 μg mL^{-1} antibody did not improve the performance significantly comparing with 10 μg mL^{-1} (data not shown), we chose 10 μg mL^{-1} to prepare the Pt–Au based Ab_1.

As most NPs-antibody requires a specific pH range for optimal response, the highest S/N ratio was obtained with pH 9–10, so this pH range was adopted as the optimal condition (Fig. S5c).

The S/N ratio also changes along with the reaction. The highest ratio was obtained after we added TMB for 10–20 min (Fig. S5d). At the beginning, the signal enhanced as times went on because of the increasing oxidation products. Then, the signal intensity flattened, which might be due to the completion of oxidative reaction and also the diffusion blurring signal. To balance, we waited for 10–20 min after adding TMB for all the experiments.

4. Conclusion

We reported a low-cost and sensitive detection method of *E. coli* O157:H7 using signal amplification strategy. The amplification principle is based on the peroxidase-like activity of bimetal NPs toward TMB solution. The measurements were performed by analyzing the color intensity with naked eyes and a portable strips reader. This approach relies on using bimetal NPs as label for reporting antibody. This new technology is a major breakthrough for real-time, sensitive, rapid, qualitative and even quantitative detection of variety of foodborne pathogen or biomarkers in diagnostics. It also has broad impacts on the health diagnostics in developing countries because of the low-cost and easy operation.

Notes

The authors declare no competing financial interest.

Acknowledgment

This work was supported by the Centers for Disease Control and Prevention/National Institute for Occupational Safety and Health (CDC/NIOSH) Grant 1R21OH010768-01A1. We thank Franceschi Microscopy & Image Center at Washington State University for TEM measurements.

Appendix A. Supplementary material

Supplementary data associated with this article can be found in the online version at http://dx.doi.org/10.1016/j.bios.2015.10.017.

References

Ataee-Esfahani, H., Imura, M., Yamauchi, Y., 2013. Angew. Chem. Int. Ed. 52, 13611–13615.
CDC, 2012a. 2015. Can be retrieved at: ⟨http://www.cdc.gov/listeria/outbreaks/cantaloupes-jensen-farms/082712/⟩.
CDC, 2012b. 2015. Can be retrieved at: ⟨http://www.cdc.gov/salmonella/typhimurium-cantaloupe-08-12/⟩.
CDC, 2006. MMWR 55, 1045–1046.
Cebula, T.A., Payne, W.L., Feng, P., 1995. J. Clin. Microbiol. 33, 248–250.
Chen, X., Gan, M., Xu, H., Chen, F., Ming, X., Xu, H., Wei, H., Xu, F., Liu, C., 2014. Food Control 46, 225–232.
Chi, X., Huang, D., Zhao, Z., Zhou, Z., Yin, Z., Gao, J., 2012. Biomaterials 33, 189–206.
Chiao, D., Shyu, R., Hu, C., Chiang, H., Tang, S., 2004. J. Chromatogr. B: Anal. Technol. Biomed. Life Sci. 809, 37–41.
Corstjens, P.L., Claudia, J., Priest, J.W., Tanke, H.J., Handali, S., 2014. Cysticercosis Working Group in Peru, 2014. PLoS Negl. Trop. Dis. 8, e2944.

Dover, J.E., Hwang, G.M., Mullen, E.H., Prorok, B.C., Suh, S., 2009. J. Microbiol. Methods 78, 10–19.
Du, D., Wang, J., Wang, L., Lu, D., Lin, Y., 2012. Anal. Chem. 84, 1380–1385.
Eksi, H., Güzel, R., Güven, B., Boyaci, I.H., Solak, A.O., 2015. Electroanalysis 27, 343–352.
FDA, 2015. 2015.
Ge, X., Asiri, A.M., Du, D., Wen, W., Wang, S., Lin, Y., 2014. TrAC, Trends Anal. Chem. 58, 31–39.
Guo, S., Wang, E., 2011. Nano Today 6, 240–264.
He, W., Liu, Y., Yuan, J., Yin, J., Wu, X., Hu, X., Zhang, K., Liu, J., Chen, C., Ji, Y., 2011. Biomaterials 32, 1139–1147.
Hu, C., Yang, D., Zhu, F., Jiang, F., Shen, S., Zhang, J., 2014. ACS Appl. Mater. Interfaces 6, 4170–4178.
Huang, C., Dostalek, J., Sessitsch, A., Knoll, W., 2011. Anal. Chem. 83, 674–677.
Imai, S., Kouda, Y., Nishihara, T., Kinoshita, M., 1993.
Jacob, M., Foster, D., Rogers, A., Balcomb, C., Shi, X., Nagaraja, T., 2013. J. Food Prot. 76, 1626–1629.
Jung, B.Y., Jung, S.C., Kweon, C.H., 2005. J. Food Prot. 68, 2140–2143.
Kalele, S.A., Kundu, A.A., Gosavi, S.W., Deobagkar, D.N., Deobagkar, D.D., Kulkarni, S. K., 2006. Small 2, 335–338.
Karakus, C., Salih, B.A., 2013. J. Immunol. Methods 396, 8–14.
Khan, W.Z., Xiang, Y., Aalsalem, M.Y., Arshad, Q., 2013. Commun. Surveys Tutor., IEEE 15, 402–427.
Kiilerich-Pedersen, K., Poulsen, C.R., Jain, T., Rozlosnik, N., 2011. Biosens. Bioelectron. 28, 386–392.
Kinoshita, Y., Niwa, H., Katayama, Y., 2015. Microbiol. Immunol. 59, 365–370.
Kirsch, J., Siltanen, C., Zhou, Q., Revzin, A., Simonian, A., 2013. Chem. Soc. Rev. 42, 8733–8768.
Lehoux, A., Ramos, L., Beaunier, P., Uribe, D.B., Dieudonné, P., Audonnet, F., Etcheberry, A., José-Yacaman, M., Remita, H., 2012. Adv. Funct. Mater. 22, 4900–4908.
Li, Y., Afrasiabi, R., Fathi, F., Wang, N., Xiang, C., Love, R., She, Z., Kraatz, H., 2014. Biosens. Bioelectron. 58, 193–199.
Li, Z., Wang, Y., Wang, J., Tang, Z., Pounds, J.G., Lin, Y., 2010. Anal. Chem. 82, 7008–7014.
Lin, Y., Wang, J., Liu, G., Wu, H., Wai, C.M., Lin, Y., 2008. Biosens. Bioelectron. 23, 1659–1665.
Liu, C., Jia, Q., Yang, C., Qiao, R., Jing, L., Wang, L., Xu, C., Gao, M., 2011. Anal. Chem. 83, 6778–6784.
Liu, G., Lin, Y., Wang, J., Wu, H., Wai, C.M., Lin, Y., 2007. Anal. Chem. 79, 7644–7653.
Liu, X., Xiang, J., Tang, Y., Zhang, X., Fu, Q., Zou, J., Lin, Y., 2012. Anal. Chim. Acta 745, 99–105.
Liu, X., Dai, Q., Austin, L., Coutts, J., Knowles, G., Zou, J., Chen, H., Huo, Q., 2008. J. Am. Chem. Soc. 130, 2780–2782.
Liu, B., Du, D., Hua, X., Yu, X., Lin, Y., 2014. Electroanalysis 26, 1214–1223.
Ma, M., Zhang, Y., Gu, N., 2011. Colloids Surf. A 373, 6–10.
Maiyalagan, T., Dong, X., Chen, P., Wang, X., 2012. J. Mater. Chem. 22, 5286–5290.
Mannoor, M.S., Tao, H., Clayton, J.D., Sengupta, A., Kaplan, D.L., Naik, R.R., Verma, N., Omenetto, F.G., McAlpine, M.C., 2012. Nat. Commun. 3, 763.
Mao, X., Baloda, M., Gurung, A.S., Lin, Y., Liu, G., 2008. Electrochem. Commun. 10, 1636–1640.
Marder, E.P., Garman, K.N., Ingram, L.A., Dunn, J.R., 2014. Foodborne Pathog. Dis. 11, 593–595.
McCollum, J., Williams, N., Beam, S., Cosgrove, S., Ettestad, P., Ghosh, T., Kimura, A., Nguyen, L., Stroika, S., Vogt, R., 2012. J. Food Prot. 75, 1759–1765.
Miranda, O.R., Li, X., Garcia-Gonzalez, L., Zhu, Z., Yan, B., Bunz, U.H., Rotello, V.M., 2011. J. Am. Chem. Soc. 133, 9650–9653.
Nabae, K., Takahashi, M., Wakui, T., Kamiya, H., Nakashima, K., Taniguchi, K., Okabe, N., 2013. Epidemiol. Infect. 141, 1897–1904.
Nagatani, N., Yuhi, T., Chikae, M., Kerman, K., Endo, T., Kobori, Y., Takata, M., Konaka, H., Namiki, M., Ushijima, H., 2006. NanoBiotechnology 2, 79–86.
Peng, D., Hu, S., Hua, Y., Xiao, Y., Li, Z., Wang, X., Bi, D., 2007. Vet. Immunol. Immunopathol. 117, 17–25.
Qi, H., Zhong, Z., Zhou, H., Deng, C., Zhu, H., Li, J., Wang, X., Li, F., 2011. Int. J. Nanomed. 6, 3033–3039.
Resch-Genger, U., Grabolle, M., Cavaliere-Jaricot, S., Nitschke, R., Nann, T., 2008. Nat. Methods 5, 763–775.
Riley, L.W., Remis, R.S., Helgerson, S.D., McGee, H.B., Wells, J.G., Davis, B.R., Hebert, R.J., Olcott, E.S., Johnson, L.M., Hargrett, N.T., 1983. N. Engl. J. Med. 308, 681–685.
Roda, A., Mirasoli, M., Roda, B., Bonvicini, F., Colliva, C., Reschiglian, P., 2012. Microchim. Acta 178, 7–28.
Sack, D.A., Sack, R.B., 1975. Infect. Immun. 11, 334–336.
Sampath, R., Hall, T.A., Massire, C., Li, F., Blyn, L.B., Eshoo, M.W., Hofstadler, S.A., Ecker, D.J., 2007. Ann. N. Y. Acad. Sci. 1102, 109–120.
Scallan, E., Hoekstra, R.M., Angulo, F.J., Tauxe, R.V., Widdowson, M., Roy, S.L., Jones, J. L., Griffin, P.M., 2011. Emerg. Infect. Dis. 17, 7–15.
Shan, S., Lai, W., Xiong, Y., Wei, H., Xu, H., 2015. J. Agric. Food Chem. 63, 745–753.
Shen, Z., Wang, J., Qiu, Z., Jin, M., Wang, X., Chen, Z., Li, J., Cao, F., 2011. Biosens. Bioelectron. 26, 3376–3381.
Shi, L., Wu, F., Wen, Y., Zhao, F., Xiang, J., Ma, L., 2015. Anal. Bioanal. Chem. 407, 529–535.
Shyu, R., Shyu, H., Liu, H., Tang, S., 2002. Toxicon 40, 255–258.
Sun, J., Ji, J., Sun, Y., Abdalhai, M.H., Zhang, Y., Sun, X., 2015. Biosens. Bioelectron. 70, 239–245.
Ulrich, G., Ziessel, R., Harriman, A., 2008. Angew. Chem. Int. Ed. 47, 1184–1201.
Vikesland, P.J., Wigginton, K.R., 2010. Environ. Sci. Technol. 44, 3656–3669.
Wang, H., Ishihara, S., Ariga, K., Yamauchi, Y., 2012a. J. Am. Chem. Soc. 134, 10819–10821.
Wang, L., Yan, R., Huo, Z., Wang, L., Zeng, J., Bao, J., Wang, X., Peng, Q., Li, Y., 2005. Angew. Chem. Int. Ed. 44, 6054–6057.
Wang, F., Jiang, L., Yang, Q., Prinyawiwatkul, W., Ge, B., 2012b. Appl. Environ. Microbiol. 78, 2727–2736.
Wang, F., Yang, Q., Qu, Y., Meng, J., Ge, B., 2014. Appl. Environ. Microbiol. 80, 2516–2525.
Wang, J., Chen, W.N., Hu, K.X., Li, W., 2006. Wei Sheng Yan Jiu 35, 439–441.
Wendel, A.M., Johnson, D.H., Sharapov, U., Grant, J., Archer, J.R., Monson, T., Koschmann, C., Davis, J.P., 2009. Clin. Infect. Dis. 48, 1079–1086.
Xiao, F., Zhao, F., Mei, D., Mo, Z., Zeng, B., 2009. Biosens. Bioelectron. 24, 3481–3486.
Xie, Q., Wu, Y., Xiong, Q., Xu, H., Xiong, Y., Liu, K., Jin, Y., Lai, W., 2014a. Biosens. Bioelectron. 54, 262–265.
Xie, Q., Wu, Y., Xiong, Q., Xu, H., Xiong, Y., Liu, K., Jin, Y., Lai, W., 2014b. Biosens. Bioelectron. 54, 262–265.
Xu, C., Wang, L., Wang, R., Wang, K., Zhang, Y., Tian, F., Ding, Y., 2009. Adv. Mater. 21, 2165–2169.
Xu, C., Wang, R., Chen, M., Zhang, Y., Ding, Y., 2010. Phys. Chem. Chem. Phys. 12, 239–246.
Yazgan, I., Noah, N.M., Toure, O., Zhang, S., Sadik, O.A., 2014. Biosens. Bioelectron. 61, 266–273.
Zeng, J., Yang, J., Lee, J.Y., Zhou, W., 2006. J. Phys. Chem. B 110, 24606–24611.
Zhang, L., Huang, Y., Wang, J., Rong, Y., Lai, W., Zhang, J., Chen, T., 2015. Langmuir 27, 13861–13867.
Zhang, P., Liu, X., Wang, C., Zhao, Y., Hua, F., Li, C., Yang, R., Zhou, L., 2014a. PloS One 9, e105305.
Zhang, W., Asiri, A.M., Liu, D., Du, D., Lin, Y., 2014b. TrAC Trends Anal. Chem. 54, 1–10.
Zhang, W., Ge, X., Tang, Y., Du, D., Liu, D., Lin, Y., 2013. Analyst 138, 5431–5436.
Zhao, X., Hilliard, L.R., Mechery, S.J., Wang, Y., Bagwe, R.P., Jin, S., Tan, W., 2004. Proc. Natl. Acad. Sci. U. S. A. 101, 15027–15032.
Zhu, C., Wen, D., Oschatz, M., Holzschuh, M., Liu, W., Herrmann, A., Simon, F., Kaskel, S., Eychmüller, A., 2015a. Small 11, 1430–1434.
Zhu, C., Du, D., Eychmüller, A., Lin, Y., 2015b. Chem. Rev. 115, 8896–8943.
Zhu, C., Yang, G., Li, H., Du, D., Lin, Y., 2015c. Anal. Chem. 87, 230–249.
Zou, Z., Du, D., Wang, J., Smith, J.N., Timchalk, C., Li, Y., Lin, Y., 2010. Anal. Chem. 82, 5125–5133.